Article

Influence of Au, Ag, and Cu Adatoms on Optical Properties of TiO₂ (110) Surface: Predictions from RT-TDDFT Calculations

Yin-Pai Lin [1], Dmitry Bocharov [1,2], Eugene A. Kotomin [1], Mikhail G. Brik [1,3,4,5,6,*] and Sergei Piskunov [1]

1   Institute of Solid State Physics, University of Latvia, Kengaraga str. 8, LV-1063 Riga, Latvia;
    in-bai.lin@cfi.lu.lv (Y.-P.L.); bocharov@cfi.lu.lv (D.B.); kotomin@cfi.lu.lv (E.A.K.); piskunov@cfi.lu.lv (S.P.)
2   Transport and Telecommunication Institute, Lomonosov str. 1, LV-1019 Riga, Latvia
3   Institute of Physics, University of Tartu, W. Ostwald str. 1, 50411 Tartu, Estonia
4   College of Sciences & CQUPT-BUL Innovation Institute, Chongqing University of Posts and
    Telecommunications, Chongqing 400065, China
5   Faculty of Science and Technology, Jan Dlugosz University, Armii Krajowej 13/15,
    PL-42200 Czestochowa, Poland
6   Academy of Romanian Scientists, Ilfov Str. 3, 050044 Bucharest, Romania
*   Correspondence: mikhail.brik@ut.ee

Abstract: In this paper, real-time time-dependent density-functional theory (RT-TDDFT) calculations are performed to analyze the optical property and charge transitions of a single noble metal atom deposited on rutile TiO₂ (110) surface. The model structures are built reflecting the equilibrium positions of deposited adatoms atop the TiO₂ surface. The absorption spectra are calculated for all model structures under study. To provide deeper insight into photo-absorption processes, the transition contribution maps are computed for the states of deposited adatoms involved in transitions. Assuming the photon energy is enough to overcome the band gap of TiO₂ (∼3 eV), the photogenerated electrons of TiO₂ seem to be partly accumulated around deposited Au atoms. In contrast, this is rarely observed for deposited Ag and Cu atoms. Based on our calculations, we have identified the transition state mechanism that is important for the design strategy of future photocatalytic materials.

Keywords: TiO₂; photocatalyst; time-dependent density functional theory; absorption spectra; transition contribution maps

1. Introduction

The utilization of solar power to produce renewable energy is the actual challenge for modern society. Therefore, people have high expectations from photocatalytic water splitting for hydrogen generation, which has been intensely studied in the last decades. Titanium dioxide (TiO₂) was reported in 1972 as a prospective material for photocatalytic water splitting [1]. TiO₂ is one of the most studied and applied photocatalytic materials with low cost, nontoxicity, stability, and diversity of applications [2–14]. The fundamental mechanism of photocatalysis water splitting is dependent on the formation of photogenerated charge. It could be divided into photo-induced charge separation, bulk and surface charge recombination, and surface charge reactions [15]. However, the wide band gap of TiO₂ (3.0–3.2 eV) is too large for effective absorption in the visible light region of the solar spectrum. To optimize the absorption for spectra visible light range and sustain the property of redox ability, one of the possible solutions is to incorporate the noble metal into TiO₂ surface layer and thus increase optical response in the visible region [2,3,15,16].

The state-of-the-art spectroscopy can analyze the electronic structure on the atomic scale, such as binding energies [17,18], as well as imaging the reactions sites [19]. Nevertheless, the technology of fabrication of catalysts still requires improvements. From the experimental point of view, the measurements of the absorption spectra of the photocatalyst are one of the useful ways to understand the efficiency of the utilization of solar power [17,18,20,21]. Due to the restrictions of fabrication, it is still difficult to experimentally

investigate the reactions of photon-induced electron transition of a single atom or small cluster on the semiconductor surfaces [3]. Thanks to the rapid development of computer technology and the growth of computing power of supercomputers around the world, theoretical calculations based on quantum chemistry and density functional theory (DFT) have become a significant instrument to fulfill the research of charge transition and photo-absorption at the atomic scale. Time-dependent DFT (TD-DFT) combined with the method of a linear combination of atomic orbitals (LCAO) allows the simulations of structures consisting of up to hundreds of noble metal atoms [22–24], providing reasonable equilibrium between the accuracy and computational time. Time propagation within LCAO TD-DFT enables the decomposition of Kohn–Sham wavefunctions to illustrate the transition states at certain energies. This approach provides a convenient tool to present the transition behavior from the occupied to unoccupied Kohn–Sham orbitals [22–25].

Recent reviews [17,18,20] show that the noble metal clusters on top of the rutile TiO_2 (110) surface indeed enhance the absorption from the visible to ultraviolet light region. The intense broad absorption lines are induced by an electron transition from the noble metal clusters forming excited states in the system. Usually, the obtained ground states for undergoing the TD-DFT are in accordance with the optimized structure or the minimal interaction of the surface models [20,26]. However, there are still some geometric structures close to the minimal energy of the equilibrium models which can still meet the converge criteria of DFT calculations. Although it can be expected that the absorption spectrum can be similar, the changed electronic orbitals due to the disparate geometry might result in the discrepancy in the scheme of localized transitions.

In this work, the optical absorption and transition contribution of the single atoms of noble metals (Au, Ag, and Cu) deposited on the rutile TiO_2 (110) surface is analyzed from first principles. As the localized surface plasmon resonances would let the noble metal cluster respond to complex Kohn–Sham decomposition [17,18,20,22–25], the single noble atom (Me_s) is adopted to avoid the complicated plasmonic effects and distinguish the unique characteristics of Au, Ag, and Cu.

This paper is arranged in the following way. In Section 2, the computational detail and applied theoretical methods are briefly described. Section 3 presents the obtained data of interaction energies of the metal atoms with the rutile TiO_2 (110) surface, the density of electronic states, and photo-absorption spectra, as well as a detailed analysis of transition contribution maps (TCM). Finally, the conclusions are provided in Section 4 of the paper.

2. Computational Details

All the simulations in this work were performed using the GPAW package [27,28] and the ASE library [29]. For electronic band structure calculations, the Gritsenko, van Leeuwen, van Lenthe, and Baerends functional with the solid-state modification (GLLB-SC) relying on Ref. [30] were used. This functional describes well the TiO_2 band structure [31] and the noble metals *d*-orbitals [22–24]. For the excited state simulation, LCAO real-time propagation TD-DFT is utilized to calculate the absorption spectrum and analyze the transition for the designed deposited adatom positions with different heights. The electronic configuration of valence electrons per atom is as follows: $O(2s^2 2p^4)$, $Ti(3s^2 3p^6 3d^2 4s^2)$, $Cu(3d^{10}4s^1)$, $Ag(4d^{10}5s^1)$, $Au(5d^{10}6s^1)$. The default GPAW dataset package 0.9.20000 was utilized for all the atoms. The double-zeta polarized (dzp) basis sets, the common parameters of GPAW for all elements, were utilized for the oxygen atoms. Due to the bad description of unoccupied *p*-orbitals, the dzp basis sets would cause the absorption peaks of silver clusters at overestimated photon energy [32]. To reliably describe the photochemical processes, the optimized double-zeta basis sets (p-valence) [32,33] were adopted for metal atoms (Ti, Cu, Ag, and Au). In p-valence basis sets, the Gaussian polarization function of dzp basis set is substituted for a bound unoccupied *p*-type orbital and split-valence wave.

Concerning the structural optimization of the rutile bulk TiO_2, the calculated lattice constants are $a_0 = b_0 = 4.647$ Å and $c_0 = 2.969$ Å, in good agreement with experiment ($a_{exp} = b_{exp} = 4.587$ Å and $c_{exp} = 2.954$ Å) [34]. The rutile TiO_2 (110) surface slab consisting

of 96 atoms (32 Ti atoms and 64 O atoms) is cut from the bulk structure along the (110) orientation having four Ti layers. The periodic boundary conditions are imposed in x–y directions. Along the z-axis on each side of the surface slab, a vacuum space of 15 Å width is set. For optimization of atomic coordinates, a grid-spacing parameter of 0.18 Å and Perdew–Burke–Ernzerh (PBE) [35] exchange-correlation functional in the generalized gradient approximation were chosen to obtain electronic densities and potentials. K-point meshes were $9 \times 6 \times 1$ for sampling the Brillouin zone based on the Monkhorst–Pack scheme. The surface was relaxed until the maximum force of the atoms was below 0.05 eV/Å. The band gap of optimized surface is 2.9 eV, as calculated using GLLB-SC functional.

To obtain the ground state for real-time propagation of LCAO-TDDFT [36], the electronic structures for the surface with and without single noble metal are calculated by using GLLB-SC functional and coarser grid 0.25 Å. For the time-propagated wave functions, the surface models are evoked by weak δ-kick of dipole electric field along each orientation of three-dimensional space in the Cartesian coordinate system. The total propagated duration was set to 500 time-steps of 20 attoseconds within 10 femtoseconds summation. The recorded time-dependent dipole moments were utilized to derive the absorption spectrum using the Fourier transform. The spectra were calculated using the Lorentzian function broadening of $\eta = 0.07$ eV.

The full absorption spectrum $S(\omega)$ consists of the spectral constituents calculated from the Kohn–Sham decomposition of occupied states to the unoccupied states (holes) $S_{occ.}^{unocc.}(\omega)$. The transition contribution map (TCM) is an illustration of electronic excitation from the occupied to unoccupied Kohn–Sham orbitals. In TCM, the weight of $S_{occ.}^{unocc.}(\omega)$ and $S(\omega)$ is expressed by scattering on Gaussian-broadened two-dimensional plots spanned by the partial density of states (PDOS) drawn below and above the Fermi level at the vertical and horizontal axes, respectively. With this presentation, the superposition of multiple occupied and unoccupied transitions for optical absorption is visualized at the assigned excitation energy. The transition areas are colored by red (positive) and blue (negative) distributions. The positive (negative) transition contribution indicates the constructive (destructive) transition contribution of the entire absorption at the corresponding photon energy. More detailed descriptions about LCAO time propagation TD-DFT and TCM can be found elsewhere [22–25]. VESTA [37] software is used to express the pseudo-wavefunction; Python packages of NumPy [38] and Matplotlib [39] are adopted to analyze data and produce figures.

3. Results and Discussion

3.1. Interaction Energies of the Me_s with the Rutile TiO_2 (110) Surface

As a first step, the geometry of the rutile TiO_2 (110) surface was optimized using DFT with the plane-wave basis set. Based on the obtained relaxed geometry, the electronic structure was calculated using LCAO method for the surface with and without deposited Me_s. The atomic structure of the surface with deposited Me_s was re-optimized. Supplementary Materials S1 show the difference between unrelaxed and optimized atomic structures. In our calculations, we fix the surface structure and place the Me_s, adjusting the distance (h) between the surface and Me_s. The outermost plane of the surface slab is positioned on the surface bridging O atoms (O_b), which is also the highest position atop the surface. The six positions of the atom location are shown in Figure 1a. Using this approach, the gradient convergence of some positions cannot be reached employing LCAO self-consistent calculations (Figure 1b,c, diagonal dashed line). The atomic structure has a large impact on the electron-hole transition from the occupied to the unoccupied state. The approximated method that we adopt in our calculations is to ensure that the predicted transitions are due to the deposited Me_s. To demonstrate the stability of each adatom position with different heights atop the rutile TiO_2 (110) surface, the interaction energies of the Me_s on the surface model were estimated as follows:

$$E_{int} = E_{(surface+atom)} - E_{surface} - E_{atom},$$

where $E_{(surface+atom)}$ is the total energy of the surface with deposited Me_s, $E_{surface}$ represents the total energy of bare rutile TiO_2 (110) surface, and E_{atom} is the total energy of Me_s. Figure 1 illustrates the interaction energy for each designed position of Me_s located close to the surface.
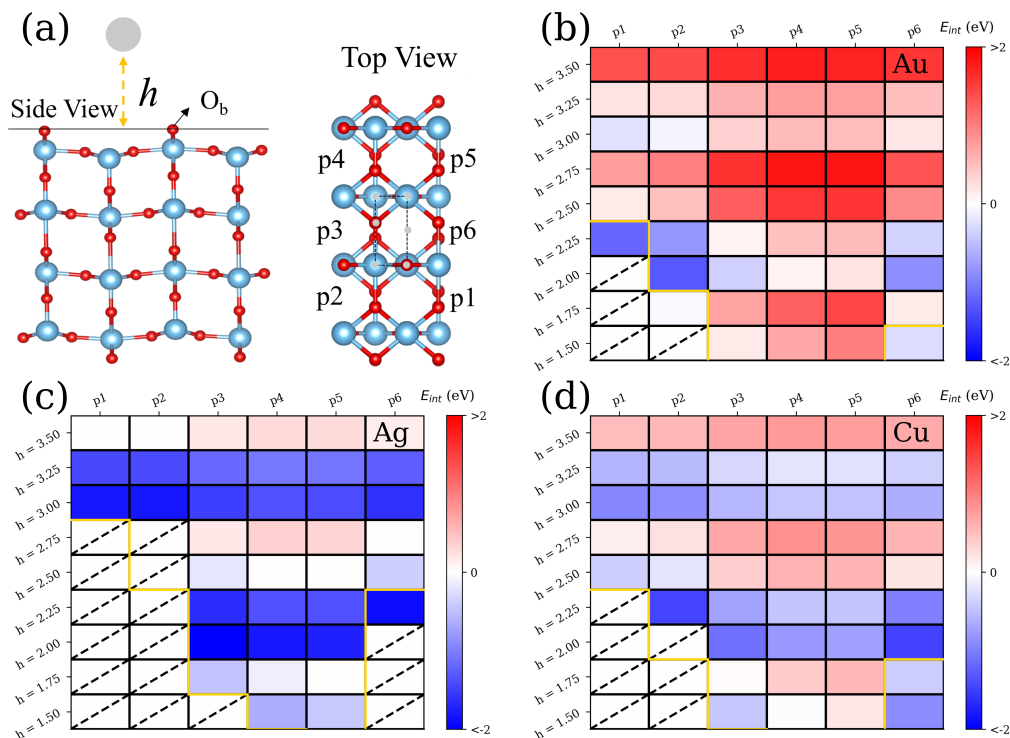

Figure 1. Schematic representation (**a**) of atomic structure of deposited Me_s on optimized rutile TiO_2 (110) surface with various height (h) at designed positions (p1 to p6). Interaction energies (E_{int}) of (**b**) Au, (**c**) Ag, and (**d**) Cu adatoms on TiO_2 surface are shown with the red–blue color pattern. The diagonal dashed-line is for the Me_s adatoms on TiO_2 surface with self-consistent field non-convergence; the yellow lines mean that there is a bond between Me_s and surrounding surface atoms.

In general, the adsorption of the Me_s atoms can be briefly separated into two types with different heights of the deposited Me_s atop the TiO_2 surface. One is the Me_s suspended atop the surface, while the other is the Me_s bonded to the surface. For the first type of deposited Me_s, as it is shown in Figure 1b,c, there is a minimum of the energy with the height at 3 Å for Au, Ag, and Cu Me_s adsorption. For this type of adsorption ($h \geq 3$ Å), the Ag and Cu surface models show larger stability at all six positions, compared to the Au surface model at the same altitude. The suspended Me_s is attracted by O_b atoms (p1, p2, and p2 positions), which means that the Me_s is tending to form the bond with O_b. On the whole, the longer the distance between the suspended Me_s and the surface, the larger the interaction energy for all six analyzed positions of adsorption.

If the deposited Me_s keeps approaching the surface ($h < 3$ Å), then interaction between the deposited Me_s and neighbor atoms on the surface increases. To simplify the analysis of O_b and Me_s, interaction oxygen atoms bonded with Me_s locating in p1, p2, and p6 positions, not in p3, p4, and p5 positions, are, respectively, considered. For the Me_s bonded to O_b, the first thing that needs to be noticed is the self-consistent field non-convergence. At the p1 and p2 positions, the non-optimized bond length between Me_s and O_b leads to the failure of self-consistency iterations for the Me_s around the O_b position. The decrease in bond length between deposited Me_s and O_b at p6 position is small in comparison to p1 and p2 positions. Therefore, the criteria of convergence for self-consistent calculations are easier to be fulfilled. For the Me_s not bonded to O_b, the behavior of deposited Me_s is similar to the previously described suspended Me_s. At p3, p4, and p5 positions, there is still another

relative minimum energy, as with the height atop the surface that is equal to 2 or 2.25 Å. The bond at this distance is obvious between Me_s and neighbor atoms.

3.2. Electronic Density of States

To better understand the influence of Me_s deposition atop the surface, the electronic densities of states (DOS) are plotted for structures calculated by means of the LCAO method. There are three types of the structures that include suspended Me_s, both suspended and bonded Me_s, and bonded Me_s. First, the DOSes of Au, Ag, and Cu adatoms on TiO_2 surface are presented at six selected positions ($h = 3$ Å) for the suspended Me_s. As for the other two types of structures, not all the six selected positions ($h < 3$ Å) are converged in the ground state calculations. Therefore, the DOSes of surface structures are secondly considered at p3, p4, and p5 positions ($h = 2$ Å), which present the circumstances of Me_s bond between suspended and bonded condition. Thirdly, the DOS projected onto atoms in the vicinity of O_b are only shown at p6 position for Au, Ag, and Cu surface structures due to the energy divergence at p1 and p2 positions in calculations of bonded Me_s states. The heights are 1.5 Å, 2.25 Å, and 1.75 Å, respectively. All the DOSes are shown in Figure 2.
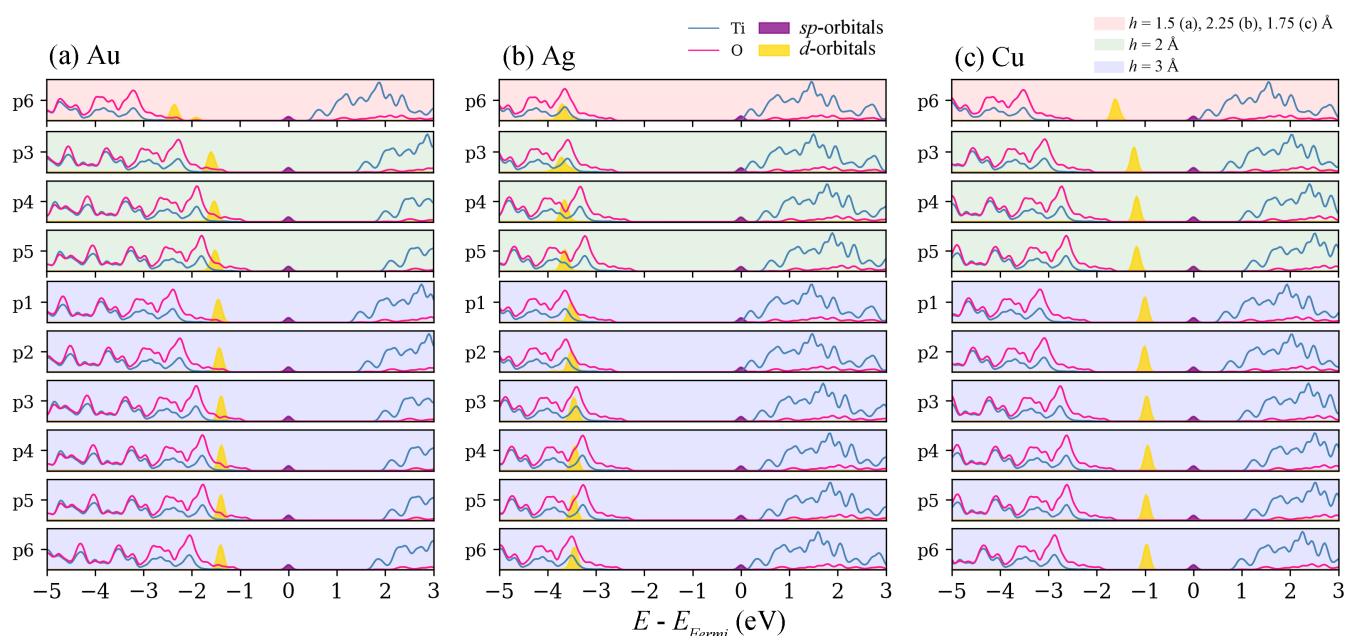

Figure 2. Density of states (DOS) of deposited Me_s on the TiO_2 surface for Au (**a**), Ag (**b**), and Cu (**c**) surface structures. The zero at energy scale is set to the Fermi level for each surface structure. Considering TiO_2, DOSes are projected to the Ti (blue line) and O (pink line), respectively. The *sp*-orbitals (purple area) and *d*-orbitals (yellow area) of Me_s are elucidated. The background color for each panel are as follows: suspended Me_s ($h = 3$ Å; light blue space), between suspended and bonded Me_s ($h = 2$ Å; light green space), and bonded Me_s ($h = 1.5$ Å for Au, 2.25 Å for Ag, and 1.75 Å for Cu; light red space), respectively.

The DOSes of Au, Ag, and Cu surface structures were calculated at the height equal to 3 Å at six designated positions. It can be seen that the DOSes of all Ti and O atoms are shown to interpret the surface states; the partial DOSes projected on Me_s *sp* and *d* orbitals are presented as well. It is also revealed that the DOS of Ti and O are of the same distributions as for Au, Ag, and Cu surface structures. The suspended Me_s is not because the TiO_2 orbitals hybridized again, which only changes the Fermi level energy for the whole system. Besides, the TiO_2 bandgap of surface is almost the same as the pure TiO_2 surface (∼2.894 eV). For *sp*-orbitals of Me_s, the energy of the Ag atom is the closest to the TiO_2 conduction band minimum (CBM). For *d*-orbitals of Me_s, the energy of the Au atom is the closest to the TiO_2 valence band maximum (VBM). The energy of Cu *sp*-orbitals

and *d*-orbitals is between the VBM and CBM of TiO_2. For the relative minimum energy (h = 2 Å), the DOS of Au, Ag, and Cu surface structures at p3, p4, and p5 positions are similar to the results of suspended Me_s, except the *d*-orbitals shifting to the lower energy.

For the Me_s bonded to surface, p6 position for Au (h = 1.5 Å), Ag (h = 2.25 Å), and Cu (h = 1.75 Å) surface structures are considered. According to the closest energy state to VBM of TiO_2, the bonded Au atom triggers the orbital of TiO_2 surface to be hybridized, causing the O_b orbitals and Au Me_s to form the band edge of the valence band. In contrast, there is no new peak or reshape for the bonded Cu atom. In addition, there is apparently a new formation peak for Ag Me_s at around −3 eV, which is the sharp slope of Ti and O DOSes.

In short, the suspended atom would not be strongly bonded to the O_b or other neighbor atoms, which reveals that the electronic structure of bare rutile TiO_2 (110) surface is similar to the surface with suspended adatom. In addition, the *d*-orbital of Me_s brings the hybridization of the surface states; the *sp*-orbitals of Me_s provide the overlap of the band edge of the surface conduction band. Based on the above mentioned, the process of deposited Me_s would trigger localized effects in the optical spectrum.

3.3. Photo-Absorption Spectrum

To gain more insight about the optical response, the photo-absorption spectrum and electron transitions induced with the process of depositing Me_s on the TiO_2 surface were analyzed. The absorption spectra are shown in Figure 3, which are based on ground state calculated electronic structure shown in Figure 2, including the three types of the Me_s bond types. It can be expected that the absorption spectrum of all surface structures inherits the characteristic peak of single Me_s and pure surface. In our calculations, the absorption peaks of single Au, Ag, and Cu adatoms are located at ∼5.9 eV, ∼4.2 eV, and ∼4.8 eV, respectively (see Supplementary Materials S2). Compared to the research reported by Lecoultre et al. [40–42], the peak of Au and Cu is slightly overestimated. In turn, the results obtained for the Ag adatom are in good agreement.

3.4. Transition Contribution Maps (TCM)

For the analysis of electronic transitions, the TCM and pseudo-wavefunction are adopted to visualize the localized transitions differences induced by the transitions from an occupied state to an unoccupied state. Since there is no strong absorption such as plasmonic resonance peak in structures under study, the energy 3.25 eV is chosen as this photon-energy, just overcoming the band gap of TiO_2, and a higher energy of 4.25 eV is taken to simulate the resonance condition of noble metals. To investigate the contribution of transitions induced by Me_s, the detailed TCMs from 3.25 eV to 4.25 eV are shown in Supplementary Materials S3, including all absorption lines of Me_s deposited on the TiO_2 surface and pure TiO_2 surface as well. In the case of suspended Me_s (h = 3 Å), the corresponding absorption lines of Au, Ag, and Cu are shown in Figure 3a–c. In detail, the obtained results are described in the following subsections, including suspended Me_s, between suspended and bonded Me_s, and bonded Me_s, at low (3.25 eV) and high (4.25 eV) excitation energy.
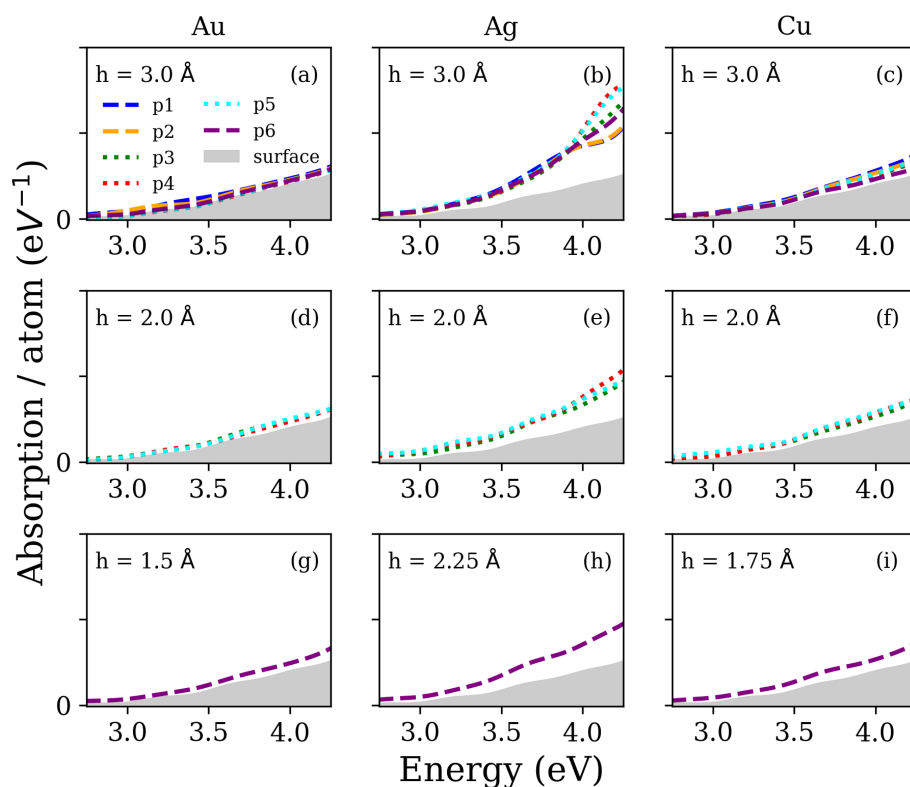
Figure 3. Photo-absorption spectra of Au (first column (**a**,**d**,**g**)), Ag (second column (**b**,**e**,**h**)), and Cu (third column (**c**,**f**,**i**)) surface structures for suspended Me_s (first row (**a**–**c**)), between suspended & bonded Me_s (second row (**d**–**f**)), and bonded Me_s (third row (**g**–**i**)). The gray area shows the absorption of the bare TiO_2 (110) surface. Blue, yellow, green, red, cyan, and purple indicate adsorption positions from p1 to p6, respectively. The dashed lines represent Me_s located around O_b; the dotted lines represent the Me_s located far from O_b.

3.4.1. TCM of Suspended Me_s (h = 3 Å) at 3.25 eV

For the case of Au, there is no obvious enhancement at this height, except the region around ∼3.25 eV, although the contribution at 3.25 eV of electron-hole transition is still controlled by TiO_2 electronic properties. Figure 4 shows the comparison of the major transition between Au and Ag at 3.25 eV. Simultaneously, there is no distinct transition for the structure with Cu surface adsorption in all positions. The transitions involving Au adatoms in almost all cases conduce to positive contributions of absorption (red) from the TiO_2 occupied states to the Au *sp*-orbitals. However, the negative contributions in absorption come not only from the occupied states of TiO_2 and Ag *d*-orbitals but also by transitions from occupied states of Ag *sp*-orbitals to the unoccupied state of TiO_2 and Ag *sp*-orbitals. The photon-induced transitions from occupied to unoccupied state contribute to the accumulated charge near Au atom at p1 and p2 positions (see insets, Figure 4). In contrast, the Ag atom becomes the supplier of charge after photon-induced transitions. There is no apparent charge accumulated around the surface Ag atom at an excited state. It indicates that the induced charge of TiO_2 would be transferred through the O_b by a suspended Au adatom. This phenomenon at 3.25 eV is the reason why the Au atom slightly triggers the enhancement of absorption at p1 and p2 positions.
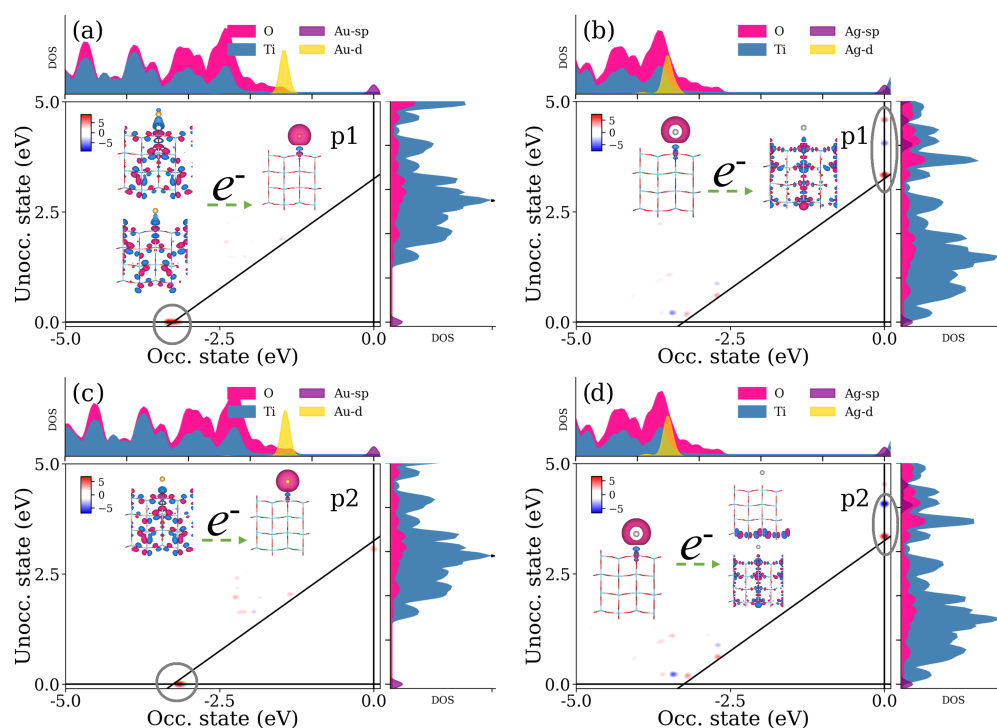
Figure 4. TCM of deposited Au (**a**,**c**) and Ag (**b**,**d**) Me$_s$ for the suspended Me$_s$ at p1 (first row, (**a**,**b**)) and p2 (second row, (**c**,**d**)) positions. The diagonal solid lines are used to emphasize the constant transition energy at 3.25 eV. DOS includes Ti, O, Me$_s$ sp-orbitals and Me$_s$ d-orbitals, which are the same as in Figure 2. The insets present the orbitals contributing in Me$_s$ charge transition, which are marked by circle (Au) and ellipse (Ag).

3.4.2. TCM of Suspended Me$_s$ (h = 3 Å) at 4.25 eV

As the photon energy moves closer to the resonance peak of the single Ag adatom (4.2 eV, Supplementary Materials S2), the surface model of Ag shows the obvious enhancement of the absorption in comparison with the model of Au and Cu. In addition, the Cu atom vaguely activates at the increments of absorption due to similar reasons. The most obvious feature is the difference at higher energy (~4.2 eV) for the surface structure with Ag, as there is a peak at p4 and p5 positions and a valley at p1 and p2 positions. The positions of deposited Me$_s$ also have an influence on the absorption. Figure 5 exhibits the TCM of Ag atom on the surface at all positions. The first column consists of p1, p2, and p6, which the O$_b$ is surrounded by; the second column is made up of p3, p4, and p5, which weakly interact with O$_b$. Initially, the transitions can be divided into TiO$_2$ contributions (square) and Ag adatom contributions (circle). Concerning the TiO$_2$ contributions, photon energy shows the major absorption of TiO$_2$ around 4.25 eV. Therefore, there are mostly positive contributions of absorption from TiO$_2$. For Ag atom contributions, Ag sp-orbitals would result in positive and negative contributions of absorption. As the Ag atom becomes closer to the O$_b$, the positive contributions are offset by the increasing negative contributions. This mechanism brings about the disappearance of the optical signature of the Ag atom, which causes a valley of absorption lines at p1 and p2 positions. Regarding the orbitals of Figure 4b,d (insets), it can be expected that there are few accumulated charges near the Ag adatom. For the TiO$_2$ contributions (square), the unoccupied state is not associated with Ag orbitals. For the Ag atom contributions (circle), the transition is based on the occupied state of Ag orbitals. Consequently, the enhancement of absorption is because of Ag atom-induced charge. The induced charge of TiO$_2$ would be merely interacted or transferred by the Ag adatom. The TCM calculated for the surface structures of between suspended & bonded Me$_s$ and bonded Me$_s$ are presented in the next subsections.
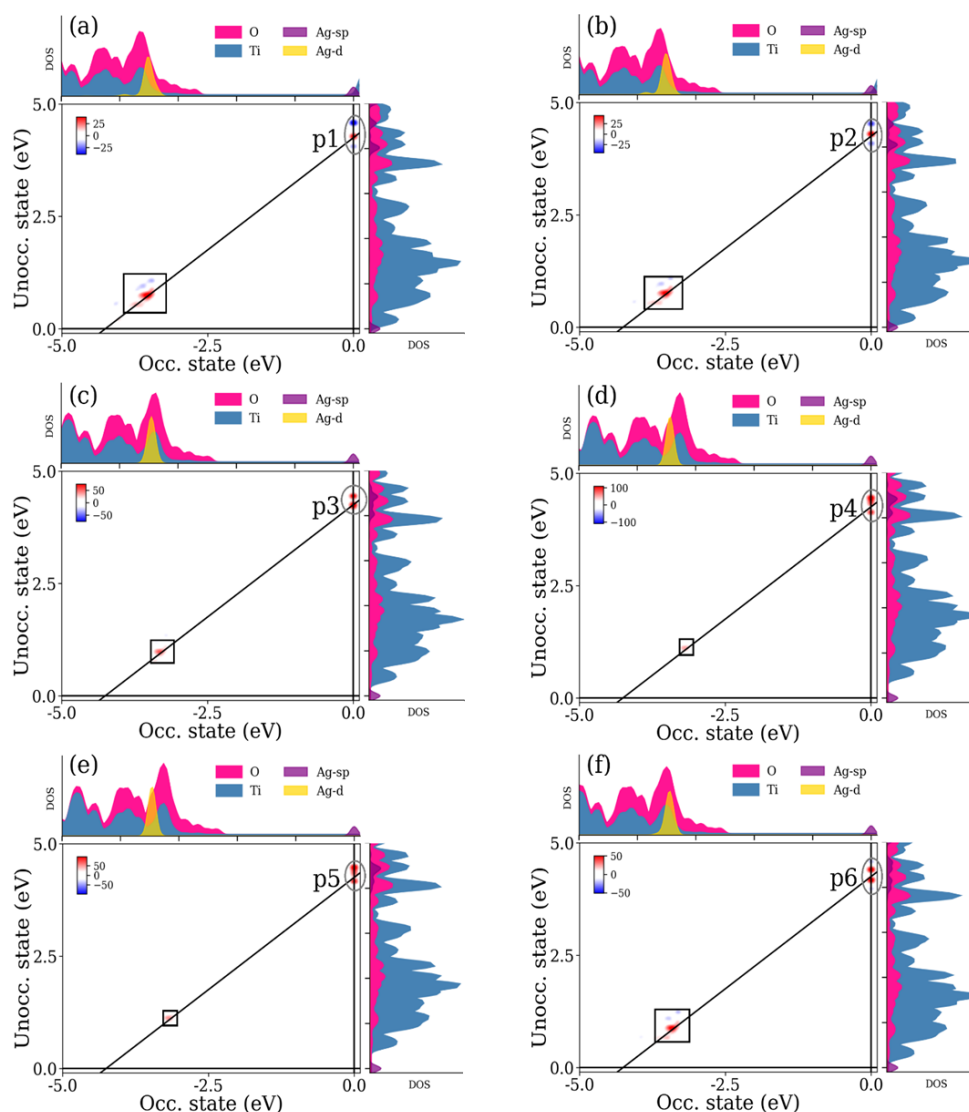
Figure 5. TCM of deposited Ag Me$_s$ for the suspended Me$_s$ at p1 (**a**), p2 (**b**), p3 (**c**), p4 (**d**), p5 (**e**), and p6 (**f**) positions. The diagonal solid lines are used to emphasize the constant transition energy at 4.25 eV. Bare TiO$_2$ contributions (square) can be found in the Supplementary Materials S3.

3.4.3. TCM of Me$_s$ between Suspended & Bonded States (h = 2 Å) at 3.25 eV and 4.25 eV

The spectra for the surface structures with Au and Cu Me$_s$ adatoms adsorbed with equilibrium distance h = 2 Å over the surface show results similar to the models with adsorption height equal to 3 Å. Nevertheless, the absorption peak at 4.25 eV seems to disappear for the Ag adatoms at p4 and p5 positions. From TCMs for the models of Ag and Cu surface adsorption (Supplementary materials, S3), it is identified that the mechanisms are analogous to the transitions from the Me$_s$ occupied state (*sp*-orbitals) to TiO$_2$ unoccupied state at 3.25 eV. In addition, the accumulated charge near Au and Cu adsorbed Me$_s$ at p3 position, which is induced by the transition from the TiO$_2$ occupied state to Au unoccupied state (*d*-orbitals), still exist at 3.25 eV (Supplementary Materials S3). Then, the Au and Cu surface adsorption models demonstrate that the transition is formed by the contribution of TiO$_2$ states at 4.25 eV. For the higher energies, the strong positive contributions of absorption are induced from the Ag occupied *sp*-orbitals to surface unoccupied state. However, the enhanced absorption for the adsorption height equal to 2 Å decreases compared to the adsorption height equal to 3 Å.

3.4.4. TCM of Bonded Me$_s$ (h$_{Au}$, h$_{Ag}$, h$_{Cu}$ = 1.5 Å, 2.25 Å, 1.75 Å, correspondingly) at 3.25 eV and 4.25 eV

In the case of Me$_s$ bonded to the surface, the optical property is still based on the TiO$_2$ surface properties. Intriguingly, TCM of Me$_s$ bonded to the surface (Figure 6) shows the intrinsic difference of transition behavior. First, the Au and Cu surface structures point to similar new electronic transitions at the lower energies. The distance between Me$_s$ (Au or Cu) and O$_b$ is far enough ($h \geq 3$ Å) that d-orbitals of Me$_s$ might not be the main transition state no matter if it is in occupied or unoccupied state. On the contrary, the d-orbitals of Me$_s$ for the case of Me$_s$ bonding become one of the occupied states for transition. Figure 6e clearly shows this phenomenon, especially for the Cu surface adsorption model. In addition, the effect of TiO$_2$ occupied states on the Au sp-orbitals transition tends to vanish. Since the length of the chemical bond is relatively short, the Me$_s$ became the part of the formed surface. The individual Me$_s$ orbitals could be redistributed by the TiO$_2$ orbitals. Therefore, the d-orbitals of bonded Me$_s$ are involved with the TiO$_2$ occupied state. This circumstance can be viewed as the noble metal atom doped into the TiO$_2$ material. Second, the Ag surface structure also shows the influence of chemical bonding at 4.25 eV, although there is no obvious reaction at 3.25 eV, owing to the bonded length not being short enough. In Figure 6d, it can be seen that the positive contribution of absorption is not as strong as the height equal to 3 Å at the p6 position. It means that the bonded Ag Me$_s$ affects the interband transition. The evidence of hybrid orbitals is the two peaks of occupied Ag d-orbitals at ~-3 eV in Figure 6c,d (DOSes, the upper panel).

Summarizing the absorption properties, there are three types of transition arising from deposited Me$_s$. First, the strongest enhancement of absorption is the transition from occupied sp-orbitals of Me$_s$ to system unoccupied state. This type of transition results in the Ag-induced charge transferring to the TiO$_2$ surface, close to the resonance peak of single Ag optical signatures. All three cases of deposited Me$_s$ could be found in this mechanism. Second, the transitions from occupied Me$_s$ d-orbitals to unoccupied state of TiO$_2$. The most obvious situation is the bonded Cu Me$_s$ at 3.25 eV in Figure 6e. As the length between Me$_s$ and O$_b$ is short enough, the optical characteristics of single Me$_s$ would be indistinct, or even be dispelled. The bonded adatoms become the doped atom in the TiO$_2$ surface. The occupied Me$_s$ d-orbitals provide new transition state at relatively low energy. Third, the transitions are formed from the TiO$_2$ occupied state to the unoccupied Me$_s$ sp-orbitals. Due to the odd number of electronic configurations for Me$_s$, it provides a single occupation at the sp-orbitals. This means that the photogenerated electrons of TiO$_2$ could accumulate around the Me$_s$. In our study, the most evident observed case is the Au Me$_s$ at the 3.25 eV without bonding to the O$_b$ in Figure 4a,c. Although the deposited Ag Me$_s$ would cause the strongest absorption, the transition is focusing on the Ag-induced charge to the unoccupied state which seems not to be the reason for harvesting the photogenerated electrons of the TiO$_2$ surface. On the other hand, deposited Au Me$_s$ could trigger the photogenerated electrons of TiO$_2$ gathering around the Au atom. For the dissociation by photogenerated electrons, this study provides another strategy that considers not only the improvements of light absorption but also the concerns about the electron transition final state. Understanding the behavior of transition in different deposited elements on the surface is especially essential to utilize the solar spectrum for future photocatalysts.
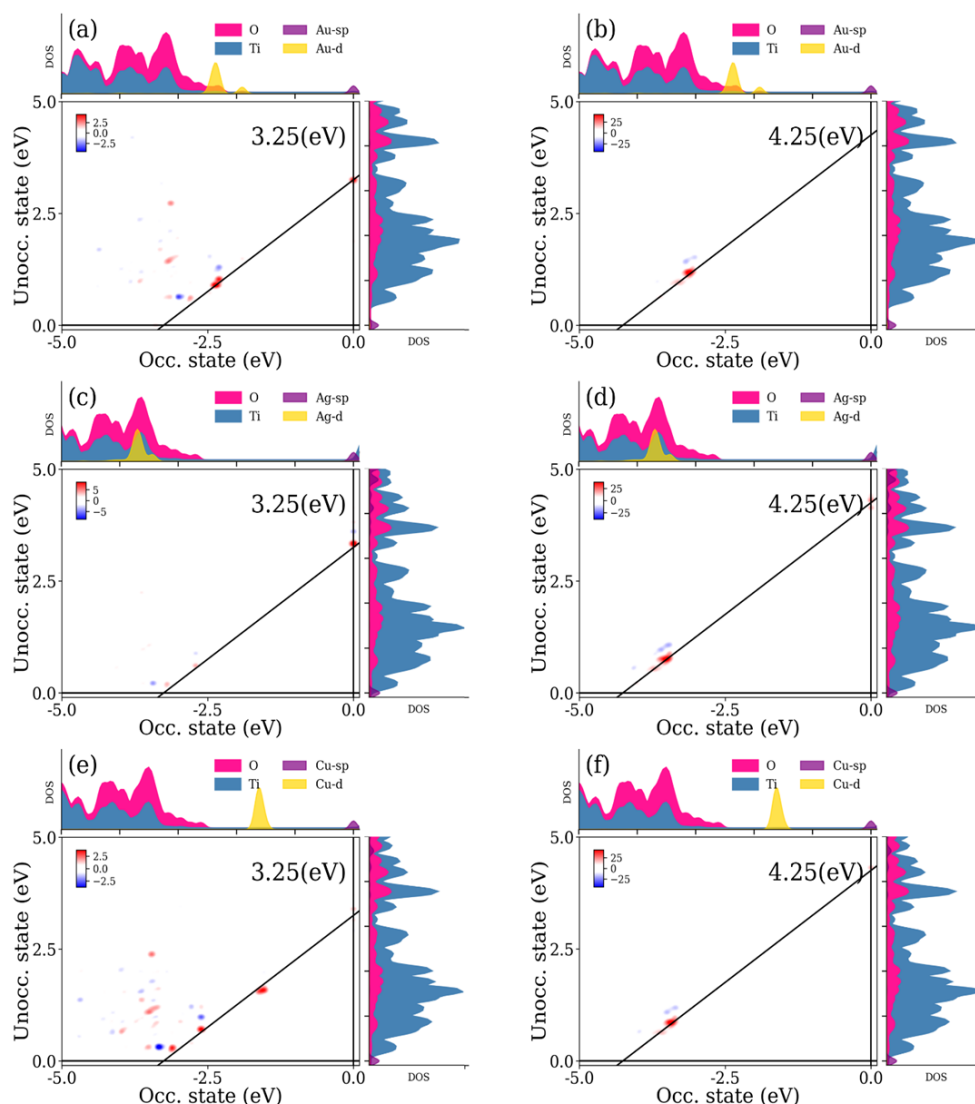
Figure 6. TCM of deposited Au (first row (**a**,**b**)), Ag (second row (**c**,**d**)), and Cu (third row (**e**,**f**)) Me$_s$ for the bonded Me$_s$ for 3.25 eV (**a**,**c**,**e**) and 4.25 eV (**b**,**d**,**f**) at p6 position. The diagonal solid lines are used to emphasize the constant transition energy.

4. Conclusions

In this study, adjusting the positions of deposited Me$_s$ within the framework of structure optimization based on the DFT self-consistent calculations guarantees the variations of optical response induced from deposited Me$_s$. First of all, the interaction energies of different positions are studied by DFT calculations. For the ground state results, the formation of deposited Me$_s$ can be divided into suspended Me$_s$, between suspended & bonded Me$_s$, and bonded Me$_s$, respectively. When the height is larger than 3 Å, the Me$_s$ is a suspended condition and tends to interact with O$_b$, which could form a relatively stable geometry. As the height is smaller than 3 Å, the energy of deposited positions near to O$_b$ are apt to diverge. In contrast, the positions not approaching O$_b$ would obtain the other relative minimum of interaction energy. Following this, the optical absorption spectra of deposited Me$_s$ on the TiO$_2$ surface are evaluated for the abovementioned three cases. For the height equal to 3 Å at 3.25 eV, the deposited Au Me$_s$ is the critical feature to harvest the charges which are generated by the photon-induced electrons from TiO$_2$ surface and transferred to Au Me$_s$. It reveals that the solar power would be efficiently applied to the photogenerated electrons of TiO$_2$ by Au Me$_s$. In the case of the height equal to 3 Å at

4.25 eV, the absorption of deposited Ag Me$_s$ shows a tremendous valley at positions around O$_b$. The close range between Ag Me$_s$ and O$_b$ causes the strong negative contribution of absorption which would decrease the total enhancement of absorption. Finally, the bonded Cu Me$_s$ at 3.25 eV shows the phenomenon of the occupied Me$_s$ *d*-orbitals to unoccupied state of TiO$_2$. It indicates that obvious bonded cases would let the optical properties of Me$_s$ disappear, and the bonded Me$_s$ can be regarded as part of the doped material of the TiO$_2$ surface. Indeed, the absorption of all three cases is similar to the convolution of each Me$_s$ and TiO$_2$ surface spectrum. However, the TCMs present more detail about the transition mechanism. Not all transitions involving noble metal provide positive contributions for absorption. In some cases, the induced charges to the unoccupied state are destructive for absorption, though the total absorption is still enhanced. For the water-splitting application, the transition manners give another design consideration for both enhancement of absorption and induced electron-hole distributions. These analyzing tools could be applied to understand the transition mechanism of photogenerated electrons in designed future catalysts and similar promising materials, e.g., SrTiO$_3$ (see Ref. [43]).

References

1. Fujishima, A.; Honda, K. Electrochemical photolysis of water at a semiconductor electrode. *Nature* **1972**, *238*, 37–38. [CrossRef]
2. Maeda, K. Photocatalytic water splitting using semiconductor particles: History and recent developments. *J. Photochem. Photobiol. C* **2011**, *12*, 237–268. [CrossRef]
3. Li, B.; Wu, S.; Gao, X. Theoretical calculation of a TiO$_2$-based photocatalyst in the field of water splitting: A review. *Nanotechnol. Rev.* **2020**, *9*, 1080–1103. [CrossRef]
4. Serga, V.; Burve, R.; Krumina, A.; Romanova, M.; Kotomin, E.A.; Popov, A.I. Extraction–pyrolytic method for TiO$_2$ polymorphs production. *Crystals* **2021**, *11*, 431. [CrossRef]

5.   Zhang, W.; Liu, H.; Liu, Z.; An, Y.; Zhong, Y.; Hu, Z.; Li, S.; Chen, Z.; Wang, S.; Sheng, X.; et al. Eu-doped zeolitic imidazolate framework-8 modified mixed-crystal TiO_2 for efficient removal of basic fuchsin from effluent. *Materials* **2021**, *14*, 7265. [CrossRef] [PubMed]

6.   Ho, V.T.T.; Chau, D.H.; Bui, K.Q.; Nguyen, N.T.T.; Tran, T.K.N.; Bach, L.G.; Truong, S.N. A high-performing nanostructured Ir doped-TiO_2 for efficient photocatalytic degradation of gaseous toluene. *Inorganics* **2022**, *10*, 29. [CrossRef]

7.   Permporn, D.; Khunphonoi, R.; Wilamat, J.; Khemthong, P.; Chirawatkul, P.; Butburee, T.; Sangkhun, W.; Wantala, K.; Grisdanurak, N.; Santatiwongchai, J.; et al.   Insight into the roles of metal loading on CO_2 photocatalytic reduction behaviors of TiO_2. *Nanomaterials* **2022**, *12*, 474. [CrossRef] [PubMed]

8.   Tsebriienko, T.; Popov, A.I. Effect of poly(titanium oxide) on the viscoelastic and thermophysical properties of interpenetrating polymer networks. *Crystals* **2021**, *11*, 794. [CrossRef]

9.   Fujishima, A.; Zhang, X.; Tryk, D.A. TiO_2 photocatalysis and related surface phenomena. *Surf. Sci. Rep.* **2008**, *63*, 515–582. [CrossRef]

10. Danish, M.S.S.; Estrella, L.L.; Alemaida, I.M.A.; Lisin, A.; Moiseev, N.; Ahmadi, M.; Nazari, M.; Wali, M.; Zaheb, H.; Senjyu, T. Photocatalytic applications of metal oxides for sustainable environmental eemediation. *Metals* **2021**, *11*, 80. [CrossRef]

11. Huang, H.; Huang, H.; Zhang, L.; Hu, P.; Ye, X.; Leung, D.Y. Enhanced degradation of gaseous benzene under vacuum ultraviolet (VUV) irradiation over TiO_2 modified by transition metals. *Chem. Eng. J.* **2015**, *259*, 534–541. [CrossRef]

12. Dong, H.; Zeng, G.; Tang, L.; Fan, C.; Zhang, C.; He, X.; He, Y. An overview on limitations of TiO_2-based particles for photocatalytic degradation of organic pollutants and the corresponding countermeasures. *Water Res.* **2015**, *79*, 128–146. [CrossRef] [PubMed]

13. Serga, V.; Burve, R.; Krumina, A.; Pankratova, V.; Popov, A.I.; Pankratov, V. Study of phase composition, photocatalytic activity, and photoluminescence of TiO_2 with Eu additive produced by the extraction-pyrolytic method. *J. Mater. Res. Technol.* **2021**, *13*, 2350–2360. [CrossRef]

14. Zhukovskii, Y.F.; Piskunov, S.; Lisovski, O.; Bocharov, D.; Evarestov, R.A. Doped 1D nanostructures of transition-metal oxides: First-principles evaluation of photocatalytic suitability. *Isr. J. Chem.* **2017**, *57*, 461–476. [CrossRef]

15. Alfaifi, B.Y.; Ullah, H.; Alfaifi, S.Y.; Tahir, A.A.; Mallick, T.K. Photoelectrochemical solar water splitting: From basic principles to advanced devices. *Veruscript Funct. Nanomater.* **2018**, *2*, BDJOC3. [CrossRef]

16. Tanabe, I.; Ozaki, Y. Far- and deep-ultraviolet spectroscopic investigations for titanium dioxide: Electronic absorption, Rayleigh scattering, and Raman spectroscopy. *J. Mater. Chem. C* **2016**, *4*, 7706–7717. [CrossRef]

17. Pilar de Lara-Castells, M.; Hauser, A.W.; Ramallo-López, J.M.; Buceta, D.; Giovanetti, L.J.; López-Quintela, M.A.; Requejo, F.G. Increasing the optical response of TiO_2 and extending it into the visible region through surface activation with highly stable Cu_5 clusters. *J. Mater. Chem. A* **2019**, *7*, 7489–7500. [CrossRef] [PubMed]

18. López-Caballero, P.; Ramallo-López, J.M.; Giovanetti, L.J.; Buceta, D.; Miret-Artés, S.; López-Quintela, M.A.; Requejo, F.G.; de Lara-Castells, M.P. Exploring the properties of Ag_5–TiO_2 interfaces: Stable surface polaron formation, UV-Vis optical response, and CO_2 photoactivation. *J. Mater. Chem. A* **2020**, *8*, 6842–6853. [CrossRef]

19. Yuan, W.; Zhu, B.; Li, X.Y.; Hansen, T.W.; Ou, Y.; Fang, K.; Yang, H.; Zhang, Z.; Wagner, J.B.; Gao, Y.; et al. Visualizing H_2O molecules reacting at TiO_2 active sites with transmission electron microscopy. *Science* **2020**, *367*, 428–430. [CrossRef] [PubMed]

20. de Lara-Castells, M.P.; Cabrillo, C.; Micha, D.A.; Mitrushchenkov, A.O.; Vazhappilly, T. Ab initio design of light absorption through silver atomic cluster decoration of TiO_2. *Phys. Chem. Chem. Phys.* **2018**, *20*, 19110–19119. [CrossRef]

21. Kenmoe, S.; Lisovski, O.; Piskunov, S.; Zhukovskii, Y.F.; Spohr, E. Electronic and optical properties of pristine, N- and S-doped water-covered TiO_2 nanotube surfaces. *J. Chem. Phys.* **2019**, *150*, 041714. [CrossRef] [PubMed]

22. Rossi, T.P.; Kuisma, M.; Puska, M.J.; Nieminen, R.M.; Erhart, P. Kohn–Sham decomposition in real-time time-dependent density-functional theory: An efficient tool for analyzing plasmonic excitations. *J. Chem. Theory Comput.* **2017**, *13*, 4779–4790. [CrossRef] [PubMed]

23. Conley, K.M.; Nayyar, N.; Rossi, T.P.; Kuisma, M.; Turkowski, V.; Puska, M.J.; Rahman, T.S. Plasmon excitations in mixed metallic nanoarrays. *ACS Nano* **2019**, *13*, 5344–5355. [CrossRef] [PubMed]

24. Rossi, T.P.; Shegai, T.; Erhart, P.; Antosiewicz, T.J. Strong plasmon-molecule coupling at the nanoscale revealed by first-principles modeling. *Nat. Commun.* **2019**, *10*, 3336. [CrossRef] [PubMed]

25. Mokkath, J.H. Strong collectivity of optical transitions in lead halide perovskite quantum dots. *Plasmonics* **2020**, *15*, 581–590. [CrossRef]

26. Qu, Z.W.; Kroes, G.J. Theoretical study of adsorption of O(3P) and H_2O on the rutile TiO_2(110) surface. *J. Phys. Chem. B* **2006**, *110*, 23306–23314. [CrossRef]

27. Enkovaara, J.; Rostgaard, C.; Mortensen, J.J.; Chen, J.; Dułak, M.; Ferrighi, L.; Gavnholt, J.; Glinsvad, C.; Haikola, V.; Hansen, H.A.; et al. Electronic structure calculations with GPAW: A real-space implementation of the projector augmented-wave method. *J. Phys. Condens. Matter* **2010**, *22*, 253202. [CrossRef]

28. Walter, M.; Häkkinen, H.; Lehtovaara, L.; Puska, M.; Enkovaara, J.; Rostgaard, C.; Mortensen, J.J. Time-dependent density-functional theory in the projector augmented-wave method. *J. Chem. Phys.* **2008**, *128*, 244101. [CrossRef]

29. Larsen, A.H.; Mortensen, J.J.; Blomqvist, J.; Castelli, I.E.; Christensen, R.; Dułak, M.; Friis, J.; Groves, M.N.; Hammer, B.; Hargus, C.; et al. The atomic simulation environment—A Python library for working with atoms. *J. Phys. Condens. Matter* **2017**, *29*, 273002. [CrossRef]

30. Kuisma, M.; Ojanen, J.; Enkovaara, J.; Rantala, T.T. Kohn-Sham potential with discontinuity for band gap materials. *Phys. Rev. B* **2010**, *82*, 115106. [CrossRef]

31. Haastrup, S.; Strange, M.; Pandey, M.; Deilmann, T.; Schmidt, P.S.; Hinsche, N.F.; Gjerding, M.N.; Torelli, D.; Larsen, P.M.; Riis-Jensen, A.C.; et al. The computational 2D materials database: High-throughput modeling and discovery of atomically thin crystals. *2D Mater.* **2018**, *5*, 042002. [CrossRef]

32. Kuisma, M.; Sakko, A.; Rossi, T.P.; Larsen, A.H.; Enkovaara, J.; Lehtovaara, L.; Rantala, T.T. Localized surface plasmon resonance in silver nanoparticles: Atomistic first-principles time-dependent density-functional theory calculations. *Phys. Rev. B* **2015**, *91*, 115431. [CrossRef]

33. Makkonen, E.; Rossi, T.P.; Larsen, A.H.; Lopez-Acevedo, O.; Rinke, P.; Kuisma, M.; Chen, X. Real-time time-dependent density functional theory implementation of electronic circular dichroism applied to nanoscale metal–organic clusters. *J. Chem. Phys.* **2021**, *154*, 114102. [CrossRef] [PubMed]

34. Burdett, J.K.; Hughbanks, T.; Miller, G.J.; Richardson, J.W.; Smith, J.V. Structural-electronic relationships in inorganic solids: Powder neutron diffraction studies of the rutile and anatase polymorphs of titanium dioxide at 15 and 295 K. *J. Am. Chem. Soc.* **1987**, *109*, 3639–3646. [CrossRef]

35. Perdew, J.P.; Burke, K.; Ernzerhof, M. Generalized gradient approximation made simple. *Phys. Rev. Lett.* **1996**, *77*, 3865–3868. [CrossRef] [PubMed]

36. Larsen, A.H.; Vanin, M.; Mortensen, J.J.; Thygesen, K.S.; Jacobsen, K.W. Localized atomic basis set in the projector augmented wave method. *Phys. Rev. B* **2009**, *80*, 195112. [CrossRef]

37. Momma, K.; Izumi, F. *VESTA3* for three-dimensional visualization of crystal, volumetric and morphology data. *J. Appl. Crystallogr.* **2011**, *44*, 1272–1276. [CrossRef]

38. van der Walt, S.; Colbert, S.C.; Varoquaux, G. The NumPy array: A structure for efficient numerical computation. *Comput. Sci. Eng.* **2011**, *13*, 22–30. [CrossRef]

39. Hunter, J.D. Matplotlib: A 2D graphics environment. *Comput. Sci. Eng.* **2007**, *9*, 90–95. [CrossRef]

40. Lecoultre, S.; Rydlo, A.; Félix, C.; Buttet, J.; Gilb, S.; Harbich, W. UV–visible absorption of small gold clusters in neon: Au_n (n = 1–5 and 7–9). *J. Chem. Phys.* **2011**, *134*, 074302. [CrossRef] [PubMed]

41. Lecoultre, S.; Rydlo, A.; Buttet, J.; Félix, C.; Gilb, S.; Harbich, W. Ultraviolet-visible absorption of small silver clusters in neon: Ag_n (n = 1–9). *J. Chem. Phys.* **2011**, *134*, 184504. [CrossRef] [PubMed]

42. Lecoultre, S.; Rydlo, A.; Félix, C.; Buttet, J.; Gilb, S.; Harbich, W. Optical absorption of small copper clusters in neon: Cu_n, (n = 1–9). *J. Chem. Phys.* **2011**, *134*, 074303. [CrossRef] [PubMed]

43. Sokolov, M.; Mastrikov, Y.A.; Zvejnieks, G.; Bocharov, D.; Kotomin, E.A.; Krasnenko, V. Water Splitting on Multifaceted $SrTiO_3$ Nanocrystals: Computational Study. *Catalysts* **2021**, *11*, 1326. [CrossRef]